ACS APPLIED MATERIALS & INTERFACES

RESEARCH ARTICLE

www.acsami.org

Interaction Stresses in Carbon Nanotube–Polymer Nanocomposites

Meysam Rahmat, Kaushik Das, and Pascal Hubert*

Department of Mechanical Engineering, McGill University, 817 Sherbrooke Street West, Montreal, Quebec, Canada H3A 2K6

ABSTRACT: A new technique of atomic force microscopy interaction measurement is used to obtain the three-dimensional stress field in nanocomposites made of single-walled carbon nanotubes (SWNT) and poly(methyl methacrylate) (PMMA) matrix. This original approach expands the current capability of AFM from imaging and force mapping to three-dimensional stress field measurements. Latest developments in the field have been limited to three-dimensional imaging at the surface only, and one value (adhesion) force mapping. The current work provides the interaction stress results for a PMMA–SWNT nanocomposite and shows a maximum estimated load transfer of less than 7 MPa (the maximum attraction stress estimated). This value is obtained for an unfunctionalized nanocomposite and hence the interaction stress is mainly based on van der Waals interactions. This means that for this system, carbon nanotubes behave similar to an elastic–fully plastic material with a yield stress of less than 7 MPa. This phenomenon illustrates why carbon nanotubes may not show their strong mechanical properties (yield strength of above 10 GPa) in polymeric nanocomposites.

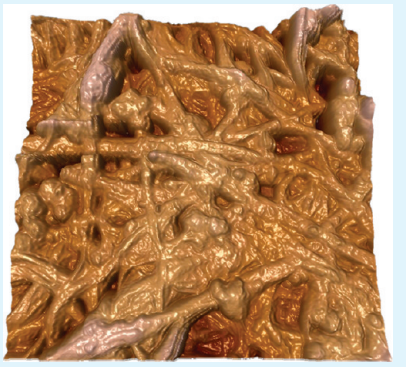

KEYWORDS: atomic force microscopy, interaction stress, single-walled carbon nanotube, poly(methyl methacrylate), nanocomposite

INTRODUCTION

Various fields of science investigate interaction problems at different scales. For example, contact mechanics deals with the interaction at the macroscale, and physical chemistry addresses this problem at the atomic level.[1] However, nanoscience encounters interaction between constituent materials at different scales, from average properties in structural nanocomposites[2] to single bond interaction between atoms.[3] Structural nanocomposites benefit from the superior properties of nanoscale reinforcements when an optimum interaction (depending on the case) between the reinforcement and matrix material is achieved. The reinforcement–matrix interaction plays an important role in dispersion of the nanoscale reinforcements[1] as well as the load transfer between the constituents.[4] Therefore, various research groups have tried to investigate the interaction parameters (e.g., interaction energy) in nanocomposites both analytically and experimentally. Typically, the modeling approaches that simulate polymer–reinforcement interactions employ Molecular Dynamics (MD) or Monte Carlo simulations. A large fraction of the modeling work in this area focuses on the carbon nanotube–polymer interaction.[5−10] Probe microscopy,[11] Raman spectroscopy,[12] dynamic mechanical analysis,[13] and X-ray diffractometry[14] have been used to investigate these interactions experimentally. Perhaps the most promising technique is atomic force microscopy (AFM) due to its high sensitivity and precision. An atomic force microscope is a powerful tool for imaging[15] and manipulating objects at the atomic scale.[16]

AFM interaction studies[17−19] cover a wide range of approaches that benefit from the small size of the AFM probe with high lateral precision and deflection sensitivity. For example, Sugimoto et al.[20] measured various interactions between known materials system and used these AFM probe–sample interactions as a fingerprint to chemically identify the type of unknown atoms in a substrate. Similarly, Ashino et al.[21] obtained the interaction force between the AFM probe and single-walled carbon nanotubes (SWNT). Thus, based on the changes in the interaction energy throughout the length of the nanotubes, they were able to locate the exact position and movement of metallofullerene molecules confined inside SWNTs.[22] In a similar fashion, Strus et al.[23] attached a carbon nanotube to the AFM probe and investigated the force required to peel it off the substrate surface. With the help of analytical modeling, the technique was used to study the interfacial energy between the carbon nanotube and different polymeric substrates.[24] Likewise, Jaiswal et al.[25] investigated the effect of surface roughness and geometry on the measured interaction forces between the AFM probe and various samples such as an alumina particle. Finally, the force measurements were used as a mapping tool to image their samples.[26]

Extensive research has been carried out on the interactions between carbon nanotube and polymer matrix over the past decade. Wagner[27−29] studied the carbon nanotube–polymer interaction using nanopull-out experiments by attaching multiwalled carbon nanotubes (MWNT) to AFM probes and using polymer films as the substrate. First, the MWNT probe was pushed in the molten polyethylene–butane. Second, the polymer was cooled and solidified around the MWNT. Finally, the probe was pulled-out while the force–displacement data were recorded. The nanotube was examined after each test to find no damage or broken polymer attached to the nanotube. The polymer substrate was also scanned to examine the hole left by the MWNT in

Received: May 21, 2011
Accepted: August 1, 2011
Published: August 01, 2011

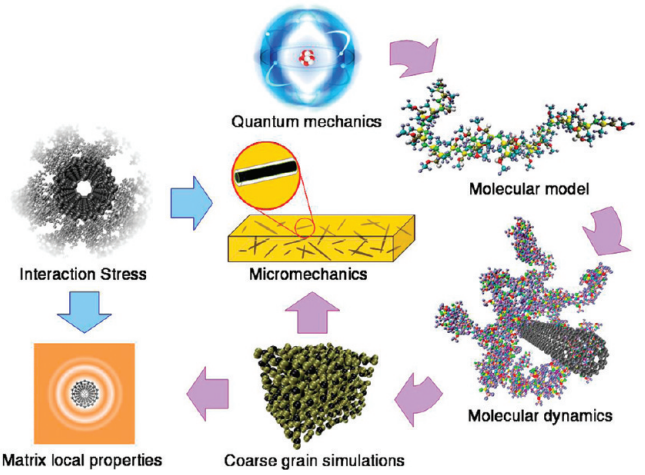

Figure 1. Multiscale approach of nanocomposite simulation. The conventional process (purple flow) starts by extracting equivalent properties of atoms (e.g., carbon atom) from quantum mechanics to be used in the molecular models. Molecular models, such as the PMMA molecule shown here, also require information about the chemical interaction of various atoms with each other, which results in the geometric properties of the molecule such as bond lengths and angles, as well as dihedrals and improper angles. A designed configuration of different molecular structures, under specific initial and boundary conditions leads to molecular dynamics simulations (e.g., a pull-out test of SWNT from PMMA chains). These simulations can be expanded into coarse grain simulations (e.g., Monte Carlo simulations). Coarse grain simulations provide local properties of matrix around the inclusion. A single-walled nanotube with the distribution function around it is shown here (horizontal purple arrow). The results of the coarse grain simulations are also used to design equivalent-continuum models, which eventually are applicable to micromechanics models such as Mori-Tanaka (vertical purple arrow). The interaction stress process eliminates the need for all the previous steps and is directly applicable to micromechanics models (horizontal blue arrow). It also generates the required data to model local properties of the polymer in the vicinity of carbon nanotubes (vertical blue arrow).

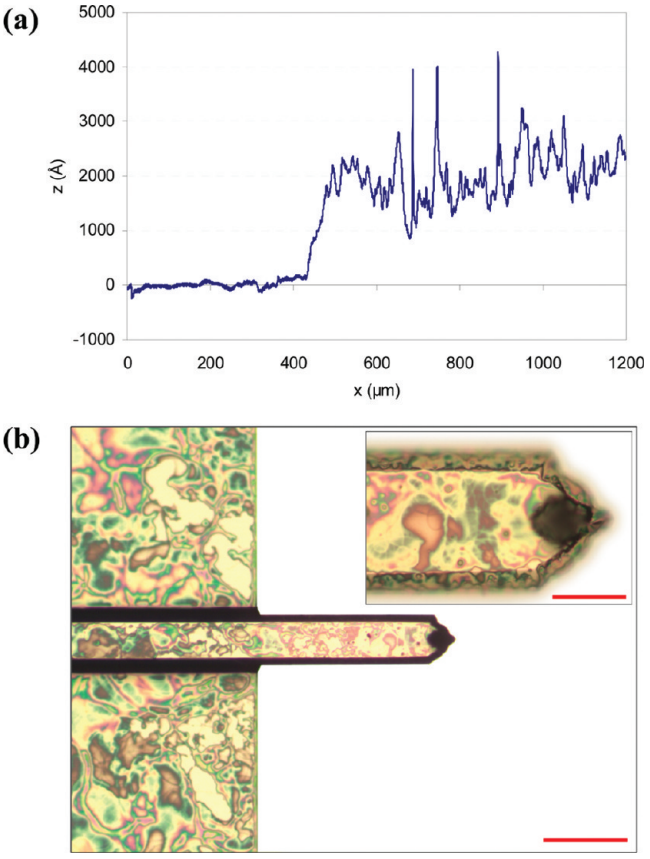

Figure 2. Surface properties of the PMMA thin film. (a) Sample of the profilometry analysis performed on a silicon wafer. A piece of masking tape was applied to the wafer before spray coating and was removed afterward as a method to measure the thickness of the PMMA thin film. The left side of the graph shows the silicon surface, which was masked by the tape during the coating, and after x = 430 μm, the profilometer scanned the PMMA thin film surface. Six lines were scanned on different locations of the silicon wafer and an average thickness of 275 $\pm$ 62 nm was measured for 20 cycles of PMMA spray coating. (b) Optical micrographs of PMMA coated AFM probes. Since performing a profilometry analysis on the actual AFM probes was not feasible, uniformity of the PMMA thin film on the AFM probes was examined using optical microscopy. The light diffraction pattern showed the existence of a PMMA layer all over the AFM cantilever. This qualitative examination was carried out before quantitative measurements using SEM. The inset shows a higher magnification of the tip. The scale bars in the main image and the inset are 100 and 30 μm, respectively.

the polymer. Given that the interaction force and the length of the MWNT were known, the interfacial fracture energy[27] and shear strength[28] were calculated. Poggi[30,31] and other researchers[32] followed the approach that used functionalized AFM probes with SWNT substrates. They performed extensive tests using thiolated AFM probes functionalized with different terminal groups, such as NH_2, CH_3, OH, SH, NO_2, and COOH. The terminal functional groups were ranked based on their interaction force with SWNT. The effect of geometry on the results was eliminated by dividing the adhesion force by the AFM probe radius.[30] Then, the functional groups concentration on the AFM probe was used to present the results in term of an adhesion force per molecule.

Even though AFM is a powerful technique, there are three main drawbacks of the AFM interaction measurement techniques: (1) unclear understanding of the interaction mechanism; (2) reporting noncomparable interaction parameters (e.g., stiction force) and (3) using ineffective procedures that limit the experimental results. As a result, a new parameter called the interaction stress was defined as "the state of stress (i.e., a tensor) at any given point of an object as a result of its vicinity to a secondary object".[33] Furthermore, it was proven that this parameter does not have the limitations of Hamaker constant (i.e., restriction to simple geometries) or Lennard-Jones potential (i.e., limited to particles). In practice, interaction stress values were obtained from AFM force−displacement curves with a novel technique called stepwise discretization method. The method was validated by performing a set of experiments and analyzing the results using Hamaker constant.

Interaction stress data, presented in this work, can be used to study local properties of the polymer at the vicinity of carbon nanotubes. This information is of high importance because the local properties of the matrix in the vicinity of inclusions (e.g., carbon nanotubes) differ from polymer bulk properties.[6] Odegard et al.[34] calculated the density of polyimide as a function of radial distance from a silica nanoparticle by inputting chemical potentials (obtained from quantum mechanics) into molecular models. As a result, coarse grain simulations provided local properties of the polymer around the nanoparticle (Figure 1).

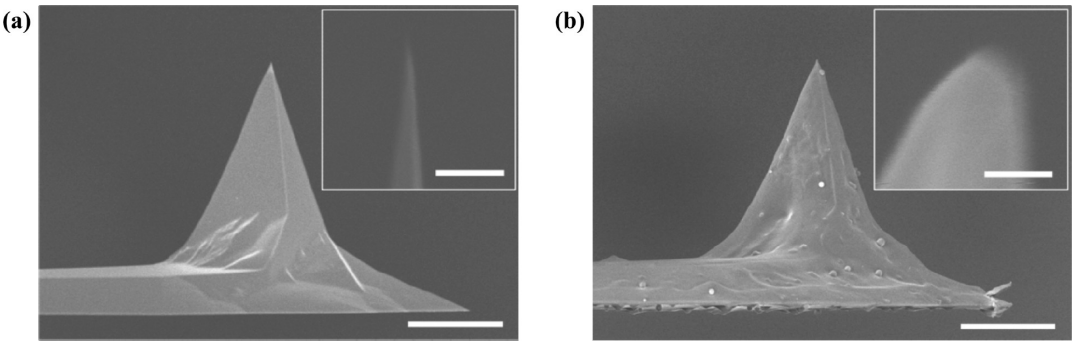

Figure 3. Scanning electron micrographs of the AFM probes. Veeco RFESP probe (a) before and (b) after PMMA coating are shown. The insets show a higher magnification of the apex. The scale bars for the main pictures and the insets are 10 μm and 100 nm, respectively. The difference between the surface topology of the probes, as well as the significant change in the diameter of the tips (insets), proves the success of the PMMA spray coating process. The image shown in b was captured after coating the PMMA coated AFM tip with a 10 nm thick layer of Au/Pl. This step is necessary to prevent the electron charging during the SEM and to result in a better quality image. However, the tip diameters of the probes were measured without Au/Pl coating. The nominal radius of 8 nm (provided by the manufacturer) was confirmed for pristine RFESP probes. An average radius of 30 nm and a flattened height of 20 nm were measured after PMMA coating (without Au/Pl layer).

The results of interaction stress, presented in the current work, can directly lead to calculating local properties of polymer around nanotubes.

Also, interaction stress can act as a shortcut to simplify the procedure of obtaining the bulk properties of nanocomposites. In order to model the bulk properties of nanocomposites, a multiscale analysis is needed. The approach proposed by Pipes and Hubert[35] consisted of a self-similar method to study the material system at different scales, such as nanoarray, nanowire, microfiber, and lamina. Odegard, Gates, Frankland, Clancy and their co-workers[34,36−38] followed an equivalent-continuum modeling approach similar to the multiscale approach presented in Figure 1. First, a representative volume element (RVE) was defined for the molecular and the equivalent-continuum models. Then, similar boundary conditions were applied to both the molecular and equivalent continuum models, and equating potential energies of deformation were derived. Next, a constitutive relationship for the equivalent-continuum model was obtained. Finally, traditional micromechanics techniques determined macroscale properties of the nanocomposite. The results found in the above-mentioned procedure can be obtained by measuring interaction stresses. The interaction stress measurements can replace the first three steps of the multiscale modeling and significantly simplify the multiscale modeling.

This paper presents the results from interaction stress measurements between PMMA and SWNT. From the results one can analyze nanocomposites at different scales and predict polymer local properties in the vicinity of carbon nanotubes. The above-mentioned applications of the interaction stress are then briefly explained in the discussion section. The interaction stress results can be applied to these problems to show how the technique deals with complicated phenomena.[39−41]

The other advantage of using interaction stress for nanocomposite applications is that it gives a three-dimensional insight of the stress level inside the material, whereas even the most recent three-dimensional AFM imaging[42] is limited to the surface topography.

RESULTS

To apply the concept of interaction stress to nanocomposites, we should bring together the two constituents, carbon nanotubes and polymeric matrix. This can be achieved through one of the two following approaches: (1) using carbon nanotube AFM probes and polymer substrates, or (2) using polymer-coated AFM probes and carbon nanotube substrates. The first approach leads to complicated force curve regimes[23,24] and defeats the purpose of simplifying the steps before micromechanics (Figure 1). Therefore, the second approach was used in this work, and the experiments were performed under distilled water to eliminate the capillary forces that result from the humidity content in the ambient air.

The functionalization of AFM probes with terminal groups was performed previously;[30−32] however, this work used AFM probes coated with complete polymer chains as opposed to solely terminal functional groups . AFM cantilevers with an optimum range of spring constant were selected. A high spring constant makes the AFM cantilever less sensitive to small forces. On the other hand, cantilevers with very low spring constants result in a jump to contact (and dynamic instability) at a greater distance from the substrate. That calls for a larger ramp size in the force curve in order to overcome the sticktion force in the retrace section and detach the AFM probe from the substrate. Furthermore, since the spring constant of the cantilever is very low, at far distances the AFM senses no attraction force, and at the smallest interaction force the cantilever jumps to contact with the substrate. This leads to a narrow window for data analysis. Hence, AFM probes with a nominal spring constant of 3 N/m were selected for polymer coating.

Poly(methyl methacrylate), also known as PMMA, was used as the polymer matrix in this work. The spray-coating technique was used to deposit the PMMA on the AFM tip with high precision. Figure 2a shows the profilometry results of the PMMA film thickness and surface roughness. An average thickness of 275 ± 62 nm was achieved using this technique. Figure 2b shows an optical micrograph of the AFM probe surface after coating. The inset shows a higher magnification of the tip. Once the probes were examined with an optical microscope, and it was confirmed that the PMMA thin film had indeed coated the AFM cantilever, scanning electron microscopy (SEM) inspection was performed. Figure 3 illustrates scanning electron micrographs of the AFM tips before and after coating. The insets show a higher magnification of the apex. It is evident that the probe with the

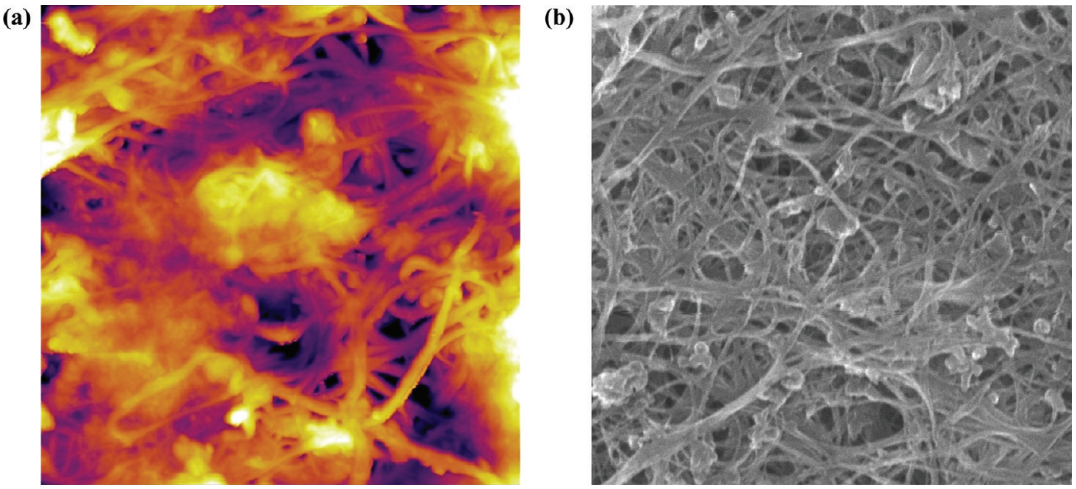

Figure 4. AFM and SEM images of the unfunctionalized SWNT buckypaper. (a) The AFM image was captured in AC mode, under ambient conditions, and at room temperature. The spectrum from white to black indicates a vertical topology range of 160 nm. SWNT bundles and impurities are distinguishable in the picture. (b) The SEM micrograph also shows the SWNT bundles with diameters in the range of 5−80 nm and particle impurities (<10 wt %). The size of both images is 2 μm × 2 μm.

initial tip radius of 8 nm is coated with a thin layer of PMMA. Unfunctionalized SWNT buckypaper, which is a mat of entangled nanotubes with high aspect ratio and random orientation, was used as the substrate. Previous studies[43,44] have reported a level of less than 10 wt % impurities in the buckypaper. Figure 4 illustrates AFM and SEM images of the SWNT buckypaper, showing randomly oriented carbon nanotubes in bundles with very high aspect ratios.

Figure 5 shows a force−position curve obtained from PMMA coated AFM probes and SWNT buckypaper substrate under distilled water. Similar force measurements with pristine AFM probes (i.e., without PMMA coating) were performed and no attraction between the tip and the substrate was observed. Negligible attraction between the tip and the substrate could be due to the small interfacial area (small tip radius), or the weak interaction between the tip material and the substrate. Given these points, it was concluded that the major contribution to the force curve shown in Figure 5 come from the PMMA−SWNT interaction, and the effect of the core of the AFM probe on the force curve was negligible. A ramp size of 100 nm was applied to the cantilever and the data from the approach regime were captured. The contact deformation and viscoelastic behavior of the polymer play important roles in the retrace regime and the value of the sticktion force.[45] Therefore, in the current work, only the approach section of the force curve was investigated. As a direct result of the AFM cantilever optimization, it is evident that a sudden jump to contact did not happen, and the force results demonstrate an acceptable precision and sensitivity. The inset in Figure 5 shows the reproducibility of the force curves, and a Gaussian distribution of the adhesion force obtained in different locations on the buckypaper surface.

The noncontact regime of the raw force curves, obtained from the AFM interaction measurements, was processed by the stepwise discretization method.[33] The data-processing procedure contained discretizing the continuous force curve into values at different steps along the force curve, defining different cross-sections for the AFM probe, and allocating the amount of force applied to each of these cross-sections. As a result of the stepwise discretization method, the stress level at each of these cross

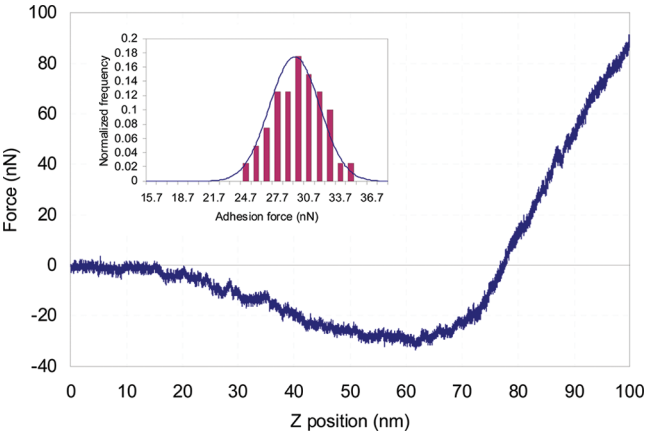

Figure 5. Raw data and repeatability of the AFM force curves. The force curve was obtained from the approach of a PMMA coated AFM probe to the SWNT buckypaper substrate under distilled water. Three regimes of noncontact, semicontact, and contact are distinguishable on the graph at 0−30, 30−75, and 75−100, respectively. The reproducibility of the force curve measurements was examined by performing 40 force curve experiments. Out of the total number of the force curves, 25 were obtained in an array of 5 × 5 on a 2 μm × 2 μm area, and the other 15 were performed randomly in a completely different area of the buckypaper. The adhesion forces (minimum value in the approach force curve) of these measurements are shown in the inset. A Gaussian distribution curve was fit to the measurements, and an average adhesion force of 29.2 nN was obtained with a standard deviation of 2.3 nN. The vertical axis of the distribution graph (inset) was normalized by dividing the number of each measurement by the total number of measurements.

sections was obtained. Figure 6 shows the interaction stress results between AFM probes coated with PMMA and a substrate made of unfunctionalized SWNTs under water. Therefore, the amount of stress induced in PMMA matrix as a result of its vicinity with SWNT can be determined as a function of distance. A maximum attraction stress (negative value) of 700 kPa at a distance of 4 nm was obtained for this material combination. The positive interaction stresses (data points at the top left corner of Figure 6a)

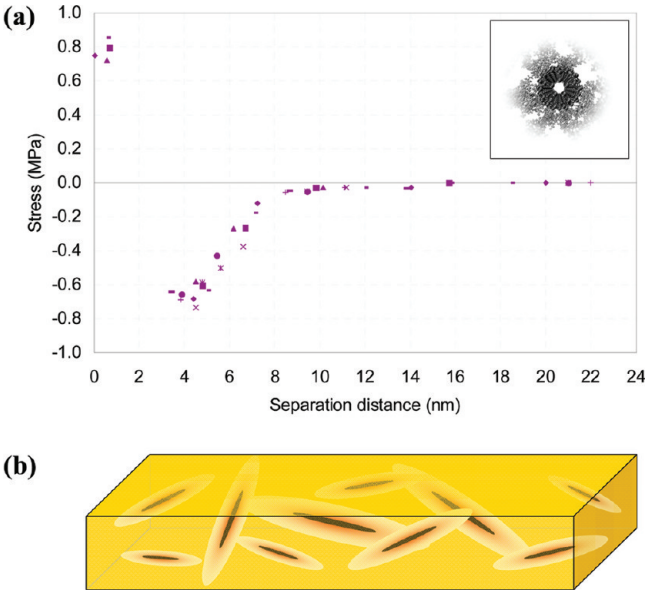

Figure 6. Interaction stress in PMMA−SWNT nanocomposites. (a) Interaction stress graph shows the amount of stress induced in a PMMA object as a result of its vicinity with a flat SWNT plane. These values were obtained based on several measurements on different locations of the SWNT buckypaper under water. In the absence of the liquid environment, it is expected to have stress values up to an order of magnitude higher. The inset shows a schematic of a SWNT surrounded by PMMA chains. The amount of interaction stress decreases significantly with separation distances above 10 nm and the nanotube does not affect the polymer chains after that. (b) Interaction stress results could be used to represent the three-dimensional stress field around bundles of SWNT in a PMMA matrix. The polymer domain which is directly influenced by the nanotube is highlighted. The details of single atom interactions with the SWNT lead to an average stress value in the polymer which is only a function of distance from the nanotube. The amount of stress applied from the nanotube reinforcements to a given section of the polymer matrix may be obtained directly from interaction stress data presented in a.

represent repulsion stresses. When the nanotube−polymer distance is less than 4 nm, the magnitude of the attraction stress decreases to reach zero, in which the nanotube and the coated tip attain the equilibrium state. At this point there is no attraction or repulsion between the nanotube and polymer. A strong repulsion was observed when the coated tip was further lowered toward the buckypaper substrate. The inflection point in the force curve (Figure 5) indicates the beginning of semicontact regime and therefore was assumed as the contact point. The separation distances (Figure 6a) were calculated according to this point.

DISCUSSION

This section begins with a comparison between the results of the interaction stress analysis and the literature. Then, further steps toward implementing the results into micromechanics models are explained. Also, the procedure of obtaining local properties of the matrix around the reinforcement is presented.

Extensive research was carried out to characterize the interfacial properties of carbon nanotube−polymer nanocomposites. The results in the literature are mainly presented in the form of interfacial shear strength[28] or interaction energy values.[27] A very wide range of interfacial shear strength from 2.7 to 376 MPa has been reported.[8,29] This is a result of using different material systems, boundary conditions, experimental or simulation approaches, assumptions, and interaction mechanisms. Therefore, a comparison between the results of the present work and the literature calls for a deeper investigation.

The nature of the forces under liquids[46] and the interaction between water and carbon based structures[47,48] are well-understood. It is known that lower electromagnetic wave velocity and smaller dipole−dipole interaction under liquids lead to smaller van der Waals interactions. That results in an increase of up an order of magnitude in the value of interaction stress when the experiment is performed under vacuum or air, instead of water or other liquids.[49] In another study, Serro et al.[50] showed that the substrate roughness significantly affected the difference between the maximum attraction force in air and under water. For a rough substrate, the maximum attraction force in air was almost equal to the value under water; whereas for a smooth substrate, the value under air was almost an order of magnitude higher. Therefore, the interaction stress value of 700 kPa, obtained under water, indicates a value of less than 7 MPa under vacuum. However, by assuming an equal value for the maximum attraction force in air and under water (i.e., similar values for work of adhesion), the maximum interaction stress in air may increase up to three times the corresponding value under water (i.e., 2.1 MPa). Frankland et al.[8] performed MD simulations of the interaction between SWNT and amorphous/crystalline polyethylene. As a result, shear strengths of 2.7 and 2.8 MPa were obtained, respectively. Moreover, they showed that formation of cross-links between less than 1% of the carbon atoms in the SWNT and the polymer led to an order of magnitude increase in the shear strength. On the other hand, Liao and Li[9] found shear strength of 160 MPa between SWNT and polystyrene in the absence of chemical bonds between the reinforcement and the matrix. However, they did not discuss the density of their matrix system in their simulation, and that significantly affects the results. Other values of shear strength in the range of 35−376 MPa were presented by Wagner and his co-workers.[27−29] They studied the pull-out of carbon nanotubes from polymers, but the interaction mechanism of the pull-out test was not completely understood. The authors suggested strengthening mechanisms such as covalent bonding between the nanotube and the polymer, or wrapping of polymer chains around the nanotubes to be the reason for such high values.

In the current work, the interaction stress data were obtained for a PMMA/H_2O/SWNT system. The results were compared with the literature by assuming a 10-fold increase in the magnitude of the stress under vacuum. The aim of the work was to demonstrate the capability of the stepwise discretization method and interaction stress data in evaluating the maximum interaction between unfunctionalized carbon nanotubes and PMMA. Therefore, a multiplication factor of 10, which is the highest value in the literature, was selected for the current work. The interaction stress data were obtained by a few different tips and the results showed to be independent of the tip. The polymer coated on a silicon wafer showed a surface roughness of ±62 nm and the coated tip diameter was different for the different tips. Therefore, a precise evaluation of the tip geometry before and after the force curve measurements was performed to ensure the quality of the coating process and measure the diameter and flatness of the coated tip.

Because the interaction stress results are within the range of values reported in the literature, they can be used as realistic inputs to micromechanical models. These results can be implemented

into micromechanical models such as Mori-Tanaka. Mori-Tanaka analysis often overpredicts the mechanical properties of nanocomposites. This is because a perfect bonding between the reinforcement and the matrix is assumed. However, in reality, the reinforcement and matrix start to slide with respect to each other when the interfacial stresses exceed the maximum interaction stress. This limits the contribution of the reinforcement to the strength of the structure. The interaction stress results show that a maximum stress of less than 7 MPa (in the absence of a third material) exists between PMMA and SWNT. It means that only 7 MPa stress can be transferred from PMMA to the SWNT and that is the maximum contribution of the nanotube to the strength of the nanocomposite. The system is equivalent to a nanocomposite with elastic−fully plastic reinforcements that yield at a stress of 7 MPa. The results of this analysis lead to a better agreement between the mechanical properties obtained from macroscale experiments, and Mori-Tanaka micromechanical models.

Furthermore, the interaction stress data can assist to calculate local properties of PMMA in the vicinity of SWNT. Two types of interaction stress graphs (PMMA−SWNT and PMMA−PMMA interaction results similar to Figure 6a) are implemented into an optimization code. The other inputs include geometry parameters such as SWNT diameter. The optimization code finds the position of the polymer chains in the equilibrium state. This is done by positioning the PMMA chains in locations that lead to the least amount of residual stress (interaction stress between PMMA and SWNT or between PMMA chains themselves). The output is the configuration of the PMMA chains around the nanotube, as well as the amount of residual stresses in the system. From the configuration of PMMA chains around the nanotube, local density of the polymer as a function of radial distance from the nanotube is obtained.

CONCLUSIONS

In the current work, the new concept of interaction stress was developed for carbon nanotube−polymer nanocomposites. From the results, the stress field inside a nanocomposite was determined as a function of distance from the reinforcing nanotubes. This led to a three-dimensional insight of the stress level inside the nanocomposite. The importance of the results is recognized when it is noticed that even the most recent three-dimensional AFM techniques merely present a topographical image of the surface and are not able to report from the inside of the samples. Direct results of the current work are applicable to multiscale modeling of nanocomposites and polymer chemistry investigations such as density evaluation and radial distribution of polymer chains around nanoinclusions. Most importantly, this work clearly demonstrated that a nanocomposite made out of PMMA and unfunctionalized SWNT was equivalent to a PMMA system with reinforcements that have yield strength of less than 7 MPa. Hence, the superior mechanical properties of SWNT can not be employed in unfunctionalized SWNT−PMMA nanocomposites, and that is why in this system, carbon nanotubes are not successful in structural applications. In the current work, a new approach to investigate the efficiency of van der Waals interaction in the absence of any functionalization technique was presented. Most of the improvements obtained in the literature benefit from the functionalization of nanotubes, and even with the functionalization, the experimental results are still well below the theoretical predictions. The goal of the current manuscript was not to criticize the current approach of functionalizing nanotubes, or to deny the improvements achieved in structural nanocomposites, but to present a new approach and investigate the influence of van der Waals interactions on the mechanical performance of carbon nanotube nanocomposites.

MATERIALS AND METHODS

Atomic Force Microscopy. The buckypaper image was taken using a Cypher atomic force microscope from Asylum Research, Santa Barbara, CA. The microscope was operated in AC mode, at room temperature and under ambient conditions. The scan rate was set to 1 Hz. For imaging, Olympus AC240TM probes were used. These probes were made of silicon and had a natural frequency of 70 kHz and a spring constant of 2 N/m.

The force curves were obtained using a Veeco Dimension V atomic force microscope from Veeco Metrology Group. The operation was performed under distilled water and at room temperature. A ramp frequency of 0.1 Hz was selected to provide the maximum resolution while preventing thermal drifting. Veeco RFESP probes with cantilever natural frequency of 62−82 kHz and nominal tip radius of 8 nm were selected to be used for force curve measurements. These probes were made of 0.01−0.025 Ω cm antimony (n) doped Si and had a nominal spring constant of 3 N/m. After coating with PMMA, the natural frequencies of the cantilevers in air and under water were in the range of 80.7−91.6 and 33.5−36.4 kHz, respectively. The quality factors of the coated probes were 252−313 in the air and 15−16 under water. The spring constants of the cantilevers after PMMA coating were calculated using Sader technique[51] and varied in the range of 5.194−7.732 N/m.

Optical Microscopy. A Nikon Eclipse L150 optical microscope was used to obtain optical micrographs of the PMMA coated AFM probes, at 100 and 500 times magnifications.

Profilometry. The thickness and surface roughness of the PMMA thin film were measured using an Ambios XP200 stylus profilometer. Six lines were scanned before an averaging led to calculating the surface roughness of the PMMA thin film.

Scanning Electron Microscopy. Scanning electron micrographs were captured using a Hitachi S-4700 FE-SEM. The system was operated at a voltage of 5 kV and a current of 10 μA for the AFM probe imaging. However, for buckypaper imaging, the setting was changed to 10 kV and 9.5 μA current in order to have a deeper penetration of the electron beam. The AFM probes were fixed on the stage by conductive carbon tape, while the buckypaper was fixed on the stage using silver paint. The diameters of the PMMA coated probes were measured without further coating, but the images shown in the paper were obtained after coating the PMMA coated AFM probes with a thin layer of Au/Pl.

Spray Coating. The PMMA layer was spray coated on the AFM probes by an EVG101 spray coater (EVGroup). The dispense rate, nozzle pressure, and ultrasonic power were maintained at 5 μL/s, 1000 mbar and 1.4 W, respectively. The spray coating parameters were optimized for a 4 wafer, and the spray coating was performed from edge-to-edge of the wafer. The wafer-stage was rotated at 80 rpm, with the direction of rotation (clockwise/counter-clockwise) changing after every cycle. The AFM cantilevers were then baked at 100 °C for 11 min on a hot plate. Similar procedure was performed on a silicon wafer to be used for profilometry. Two sets of 20 and 30 cycles of coating were performed on two sets of AFM probes.

Sputter Coating. SEM micrographs of the PMMA coated AFM probes were obtained after coating the probes with a 10 nm thick layer of gold/palladium. This layer was deposited on the PMMA coated probes by using a Hummer VI sputter coater. A vacuum level of 25 mTorr was maintained in the chamber before filling it with argon at a stable pressure of 70 mTorr. The coating was achieved after 1 min sputtering at a current of 10 mA.

PMMA. Higher MW of the polymer chains leads to a better load transfer in nanocomposites.[2] Thus, in the current work 950k PMMA A2 (Microchem Inc.) solution was used. The solution consisted of 2 wt % PMMA in anisole, and was further diluted with methyl isobutyl ketone (MIBK) so as to reduce the viscosity of the resist and to make it amenable for spray coating. The diluted resist solution contained MIBK and anisole in weight ratio of 3:1.

SWNT Buckypaper. Unfunctionalized SWNT buckypapers were provided by National Research Council Canada-Steacie Institute for Molecular Sciences (NRC-SIMS). They were manufactured using the laser oven technique.[43,44] A purification procedure containing cycles of solvent extraction, floatation, and precipitation was followed to decrease the impurity level below 10 wt %.

AUTHOR INFORMATION

Corresponding Author

*Address: Macdonald Engineering Building, Room 367, 817 Sherbrooke Street West, Montreal, Quebec, Canada H3A 2K6. Tel: (514) 398-6303. Fax: (514) 398-7365. E-mail: pascal.hubert@mcgill.ca.

ACKNOWLEDGMENT

Financial support from McGill University and Chemical, Biological, Radiological and Nuclear (CBRN) Research and Technology Initiative (CRTI), project CRTI107-121RD, are acknowledged. The SWNT buckypapers were kindly provided by National Research Council Canada-Steacie Institute for Molecular Sciences (NRC-SIMS). The authors also appreciate the assistance of Amir Moshar from Asylum Research as well as Erin Quinlan and James Kratz from the Structures and Composite Materials Laboratory at McGill University.

REFERENCES

(1) Nish, A.; Hwang, J.-Y.; Doig, J.; Nicholas, R. J. *Nat. Nanotechnol.* **2007**, *2*, 640.
(2) Mu, M.; Winey, K. I. *J. Phys. Chem. C* **2007**, *111*, 17923.
(3) Friddle, R. W.; Lemieux, M. C.; Cicero, G.; Artyukhin, A. B.; Tsukruk, V. V.; Grossman, J. C.; Galli, G.; Noy, A. *Nat. Nanotechnol.* **2007**, *2*, 692.
(4) Ramanathan, T.; Abdala, A. A.; Stankovich, S.; Dikin, D. A.; Herrera Alonso, M.; Piner, R. D.; Adamson, D. H.; Schniepp, H. C.; ChenX; Ruoff, R. S.; Nguyen, S. T.; Aksay, I. A.; Prud'Homme, R. K.; Brinson, L. C. *Nat. Nanotechnol.* **2008**, *3*, 327.
(5) Gou, J.; Liang, Z.; Zhang, C.; Wang, B. *Composites, Part B* **2005**, *36*, 524.
(6) in het Panhuis, M.; Maiti, A.; Dalton, A. B.; van den Noort, A.; Coleman, J. N.; McCarthy, B.; Blau, W. J. *J. Phys. Chem. B* **2003**, *107*, 478.
(7) Frankland, S. J. V.; Harik, V. M. *Surf. Sci.* **2003**, *525*, 103–108.
(8) Frankland, S. J. V.; Caglar, A.; Brenner, D. W.; Griebel, M. *J. Phys. Chem. B* **2002**, *106*, 3046.
(9) Liao, K.; Li, S. *Appl. Phys. Lett.* **2001**, *79*, 4225.
(10) Liang, Z.; Gou, J.; Zhang, C.; Wang, B.; Kramer, L. *Mater. Sci. Eng., A* **2004**, *365*, 228.
(11) Gross, L.; Mohn, F.; Moll, N.; Meyer, G.; Ebel, R.; Abdel-Mageed, W. M.; Jaspars, M. *Nat. Chem.* **2010**, *2*, 821.
(12) Qing, Z.; Wagner, H. D. *Philos. Trans. R. Soc., A* **2004**, *362*, 2407.
(13) Lopez-Manchado, M. A.; Biagiotti, J.; Valentini, L.; Kenny, J. M. *J. Appl. Polym. Sci.* **2004**, *92*, 3394.
(14) Chang, T. E.; Jensen, L. R.; Kisliuk, A.; Pipes, R. B.; Pyrz, R.; Sokolov, A. P. *Polymer* **2005**, *46*, 439.
(15) Gross, L.; Mohn, F.; Moll, N.; Liljeroth, P.; Meyer, G. *Science* **2009**, *325*, 1110–1114.
(16) Sugimoto, Y.; Pou, P.; Custance, O.; Jelinek, P.; Abe, M.; Perez, R.; Morita, S. *Science* **2008**, *322*, 413–417.
(17) Decossas, S.; Cappello, G.; Poignant, G.; Patrone, L.; Bonnot, A. M.; Comin, F.; Chevrier, J. *Europhys. Lett.* **2001**, *53*, 742.
(18) Meurk, A.; Luckham, P. F.; Bergstrom, L. *Langmuir* **1997**, *13*, 3896.
(19) Sun, Y.; Walker, G. C. *Langmuir* **2005**, *21*, 8694.
(20) Sugimoto, Y.; Pou, P.; Abe, M.; Jelinek, P.; Perez, R.; Morita, S.; Custance, O. *Nature* **2007**, *446*, 64.
(21) Ashino, M.; Schwarz, A.; Behnke, T.; Wiesendanger, R. *Phys. Rev. Lett.* **2004**, *93*, 136101.
(22) Ashino, M.; Obergfell, D.; Haluska, M.; Yang, S.; Khlobystov, A. N.; Roth, S.; Wiesendanger, R. *Nat. Nanotechnol.* **2008**, *3*, 337.
(23) Strus, M. C.; Zalamea, L.; Raman, A.; Pipes, R. B.; Nguyen, C. V.; Stach, E. A. *Nano Lett.* **2008**, *8*, 544.
(24) Strus, M. C.; Cano, C. I.; Byron Pipes, R.; Nguyen, C. V.; Raman, A. *Compos. Sci. Technol.* **2009**, *69*, 1580.
(25) Jaiswal, R. P.; Kumar, G.; Kilroy, C. M.; Beaudoin, S. P. *Langmuir* **2009**, *25*, 10612.
(26) Voitchovsky, K.; Kuna, J. J.; Contera, S. A.; Tosatti, E.; Stellacci, F. *Nat. Nanotechnol.* **2010**, *5*, 401.
(27) Barber, A. H.; Cohen, S. R.; Kenig, S.; Wagner, H. D. *Compos. Sci. Technol.* **2004**, *64*, 2283.
(28) Barber, A. H.; Cohen, S. R.; Wagner, H. D. *Appl. Phys. Lett.* **2003**, *82*, 4140.
(29) Cooper, C. A.; Cohen, S. R.; Barber, A. H.; Wagner, H. D. *Appl. Phys. Lett.* **2002**, *81*, 3873.
(30) Poggi, M. A.; Bottomley, L. A.; Lillehei, P. T. *Nano Lett.* **2004**, *4*, 61.
(31) Poggi, M. A.; Lillehei, P. T.; Bottomley, L. A. *Chem. Mater.* **2005**, *17*, 4289.
(32) Xiaojun, L.; Wei, C.; Qiwen, Z.; Liming, D.; Sowards, L.; Pender, M.; Naik, R. R. *J. Phys. Chem. B* **2006**, *110*, 12621.
(33) Rahmat, M.; Hubert, P. *J. Phys. Chem. C* **2010**, *114*, 15029.
(34) Odegard, G. M.; Clancy, T. C.; Gates, T. S. *Polymer* **2005**, *46*, 553.
(35) Odegard, G. M.; Pipes, R. B.; Hubert, P. *Compos. Sci. Technol.* **2004**, *64*, 1011.
(36) Gates, T. S.; Odegard, G. M.; Frankland, S. J. V.; Clancy, T. C. *Compos. Sci. Technol.* **2005**, *65*, 2416.
(37) Odegard, G. M.; Gates, T. S.; Wise, K. E.; Park, C.; Siochi, E. J. *Compos. Sci. Technol.* **2003**, *63*, 1671.
(38) Odegard, G. M.; Gates, T. S. *J. Intell. Mater. Syst. Struct.* **2006**, *17*, 239.
(39) Girifalco, L. A.; Hodak, M.; Lee, R. S. *Phys. Rev. B: Condens. Matter Mater. Phys.* **2000**, *62*, 13104.
(40) Frankland, S. J. V.; Harik, V. M.; Odegard, G. M.; Brenner, D. W.; Gates, T. S. *Compos. Sci. Technol.* **2003**, *63*, 1655.
(41) Barber, A. H.; Cohen, S. R.; Wagner, H. D. *Nano Lett.* **2004**, *4*, 1439.
(42) Fukuma, T.; Ueda, Y.; Yoshioka, S.; Asakawa, H. *Phys. Rev. Lett.* **2010**, *104*, 016101.
(43) Ashrafi, B.; Guan, J.; Mirjalili, V.; Hubert, P.; Simard, B.; Johnston, A. *Composites, Part A* **2010**, *41*, 1184.
(44) Kingston, C. T.; Jakubek, Z. J.; Dénommée, S.; Simard, B. *Carbon* **2004**, *42*, 1657.
(45) Derjaguin, B. V.; Muller, V. M.; Toporov, Y. P. *J. Colloid Interface Sci.* **1975**, *53*, 314.
(46) Israelachvili, J. N.; McGuiggan, P. M. *Science* **1988**, *241*, 795–800.
(47) Werder, T.; Walther, J. H.; Jaffe, R. L.; Halicioglu, T.; Koumoutsakos, P. *J. Phys. Chem. B* **2003**, *107*, 1345.
(48) Chabrier, D.; Bhushan, B.; Marsaudon, S. *Appl. Surf. Sci.* **2010**, *256*, 4672.
(49) Goodman, F. O.; Garcia, N. *Phys. Rev. B: Condens. Matter Mater. Phys.* **1991**, *43*, 4728.
(50) Serro, A. P.; Colaço, R.; Saramago, B. *J. Colloid Interface Sci.* **2008**, *325*, 573.
(51) Sader, J. E.; Chon, J. W. M.; Mulvaney, P. *Rev. Sci. Instrum.* **1999**, *70*, 3967.